Inorganic Chemistry

ARTICLE

pubs.acs.org/IC

Hydrogen-Bonded Assemblies of Two-Electron Reduced Mixed-Valence $[XMo_{12}O_{40}]$ (X = P and Si) with *p*-Phenylenediamines

Tomoyuki Akutagawa,*[,†] Fumito Kudo,[‡] Ryo Tsunashima,[∥] Shin-ichiro Noro,[§,‡] Leroy Cronin,*[,∥] and Takayoshi Nakamura*[,§,‡]

[†]Institute of Multidisciplinary Research for Advanced Materials (IMRAS), Tohoku University, 2-1-1 Katahira, Aoba-ku, Sendai 980-8577, Japan

[‡]Graduate School of Environmental Earth Science, Hokkaido University, Sapporo 060-0810, Japan

[§]Research Institute for Electronic Science, Hokkaido University, Sapporo 001-0020, Japan

[∥]WestCHEM, Department of Chemistry, University of Glasgow, Glasgow G12 8QQ, U.K.

Supporting Information

ABSTRACT: Hydrogen-bonded assemblies of the two-electron reduced mixed-valence Keggin clusters $[PMo_{12}O_{40}]^{5-}$ and $[SiMo_{12}O_{40}]^{6-}$ were obtained by the one-pot electron-transfer reactions between *p*-phenylenediamine (PPD) or 2,3,5,6-tetramethyl-PPD (TMPPD) (donors) and $H^+_3[PMo_{12}O_{40}]^{3-}$ or $H^+_4[SiMo_{12}O_{40}]^{4-}$ (acceptors) in CH_3CN. The redox states of the $[PMo_{12}O_{40}]^{5-}$ and $[SiMo_{12}O_{40}]^{6-}$ clusters were confirmed by the redox titrations and electronic absorption measurements. In $(HPPD^+)_3(H^+)_2[PMo_{12}O_{40}]^{5-}(CH_3CN)_{3-6}$ (**1**), the N−H ∼ O hydrogen-bonded interactions between the monoprotonated $HPPD^+$ (or diprotonated $H2PPD^{2+}$) and the $[PMo_{12}O_{40}]^{5-}$ resulted in a windmill-like assembly and hydrophilic one-dimensional channels are formed with a cross-sectional area of 0.065 nm^2, and these are filled by the CH_3CN molecules. Also, the CH_3CN molecules in salt **1** were removed by immersing the single crystals of **1** into H_2O, CH_3OH, and C_2H_5OH solvents. In the compound, $(HTMPPD^+)_6[SiMo_{12}O_{40}]^{6-}(CH_3CN)_6$ (**2**), the N−H ∼ O hydrogen-bonded interactions between the monoprotonated $HTMPPD^+$ molecules and the $[SiMo_{12}O_{40}]^{6-}$ formed a "Saturn-ring"-like assembly. Each Saturn-ring was arranged into an hexagonally packed array via hydrogen-bonded and π−stacking interactions of $HTMPPD^+$, while the CH_3CN solvent present in salt **2** are only found in the zero-dimensional isolated cavities.

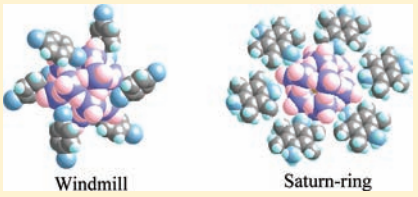

INTRODUCTION

Hydrogen-bonded interactions can play a vital role in defining supramolecular assemblies both in solution and the solid state.[1] Although the precise, predetermined, structural control of assemblies constructed using hydrogen-bonded interactions is still far from reach in global sense, the local molecular orientations determined by the intermolecular hydrogen-bonding interactions are often predictable and are controlled by utilizing functional groups of −OH, $-NH_2$, −COOH and so on.[1,2] On the other hand, the arrangement of charged molecules in solid state crystalline arrays are mainly dominated by the electrostatic interaction between the cationic and the anionic species, so that the gain of the lattice/Madelung energy can be maximized by the system.[3] In this category, polyoxometalate (POM) clusters show a rich range of complex and interesting structures with a bewildering variety of molecular-assemblies and motifs due to the size and shape and possibility to adopt one of many possible charge states.[4] The charged states of the POM-based polyanions can widely vary from $[Mo_6O_{19}]^{2-}$, $[Mo_7O_{24}]^{6-}$, $[Mo_8O_{26}]^{4-}$, $[Mo_{10}O_{34}]^{8-}$, and $[PMo_{12}O_{40}]^{3-}$, to $[Mo_{154}O_{462}H^+_8(H_2O)_{90}]^{20-}$, which strongly affects the packing structures of POMs in the crystals depending on the size and valence of counter-cations.[4,5] Keggin-type molybdenum clusters of $[XMo_{12}O_{40}]$ (X = S, P, Si, As, etc.) have a spherical molecular structure with a diameter of ∼1 nm (Scheme 1), which are one of the appropriate candidates to examine the POM assembly structures in solids. In the $[XMo_{12}O_{40}]$, two kinds of oxygen atoms (24 metal-bridging Mo−O_a−Mo and 12 terminal Mo=O_b) can contribute to the intermolecular hydrogen-bonds, which can contribute to form a variety of molecular-assembly structures in solids. Several

Scheme 1. Molecular Structures of PPD, TMPPD, and $[XMo_{12}O_{40}]$ (X = P and Si)[a]

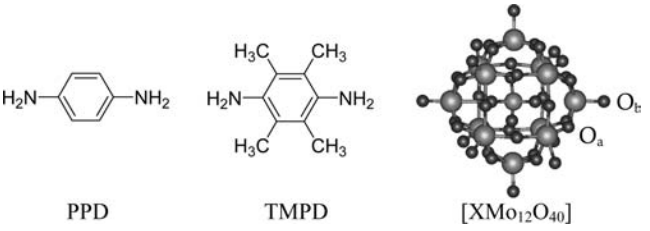

[a] The metal bridging Mo−O_a−Mo and terminal Mo = O_b oxygen sites are shown in $[XMo_{12}O_{40}]$.

Received: April 3, 2011
Published: June 14, 2011

attempts to construct one-, two-, and three-dimensional $[XMo_{12}O_{40}]$ arrangements have been reported using the organic molecules and transition metal (rare-earth metal) coordination compounds.[6−9]

One route to access the multiple-charge states of the POMs is via the stepwise reduction of the cluster via multiple electron-transfer processes, which often generates a cluster with mixed-valence electronic ground state.[4] For example, the Keggin ion $[XMo_{12}O_{40}]^{n-}$ (n = 3 for X = P and n = 4 for X = Si) can adopt charge states from n- to (n + 3)- through the multistep reduction processes,[4] where for example, the one- and two-electron reductions of $[PMo_{12}O_{40}]^{3-}$ generate one and two S = 1/2 spins on $[PMo_{12}O_{40}]^{4-}$ and $[PMo_{12}O_{40}]^{5-}$, respectively.[4,10−12] Although a large number of $[PMo_{12}O_{40}]^{n-}$ and $[SiMo_{12}O_{40}]^{n-}$ -based crystalline assemblies have been previously characterized,[6−8] those based upon the mixed-valence $[PMo_{12}O_{40}]^{5-}$ and $[SiMo_{12}O_{40}]^{6-}$ clusters are limited,[11,12] especially for the two-electron reduced species.[11,12] However these are interesting from an electronic and self-assembly point of view since the assemblies of two-electron reduced $[XMo_{12}O_{40}]^{(n+2)-}$ have the potential to form entirely different architectures from those of the $[XMo_{12}O_{40}]^{n-}$ because of the presence of stronger electrostatic interactions. Although the electrostatic interactions are the single most significant factor determining the structure of ionic lattice, the simultaneous engineering of hydrogen-bonded interaction between polyanions and organic cations should allow the development of more intricate organic−inorganic hybrids with the promise of enhanced and predetermined properties.[13] From these points of view, we selected *p*-phenylenediamine (PPD) derivatives as organic cations with hydrogen-bonding ability. In addition, PPDs possess the abilities to both accept protons and donate electrons, which will affect the proton- and electron-transfer reactions upon combination with the classical Keggin clusters of the type $[PMo_{12}O_{40}]^{3-}$ and $[SiMo_{12}O_{40}]^{4-}$.

The design of electrostatically assembled cluster architectures to form functional materials using POMs has been achieved, for example, in the area of small molecule absorption, as shown by MOF-like architectures reported based on $[XMo_{12}O_{40}]^{n-}$ with metallo-macrocations,[9] and the construction of such a porous structure using the mixed-valence $[PMo_{12}O_{40}]^{4-}$ and/or $[SiMo_{12}O_{40}]^{5-}$ assemblies have not been reported thus far, to the best of our knowledge. Since some mixed-valence POMs have paramagnetic ground states, magnetic MOFs have the potential to demonstrate interesting molecular adsorption-desorption properties associated with the paramagnetic aspects, in addition to dielectric and optical responses. For instance, the single-electron reduced $[PMo_{12}O_{40}]^{4-}$ and $[SiMo_{12}O_{40}]^{5-}$ clusters have thermally activated S = 1/2 spin ground-state, showing spin dynamics at temperatures above 60 K from the linewidth changes in the electron spin resonance spectra.[14] The spin dynamics within the two-electron reduced $[PMo_{12}O_{40}]^{5-}$ and $[SiMo_{12}O_{40}]^{6-}$ are expected to be more complicated because of the antiferromagnetic coupling of the two S = 1/2 spins on the cluster.[15] Herein, we report new hydrogen-bonding organic-inorganic hybrids between the redox active organic cations of PPD and/or 2,3,5,6-tetramethyl-PPD (TMPPD) and $[PMo_{12}O_{40}]^{5-}$ and/or $[SiMo_{12}O_{40}]^{6-}$. Since the $[PMo_{12}O_{40}]^{5-}$ and $[SiMo_{12}O_{40}]^{6-}$ clusters are highly symmetrical, highly symmetrical hydrogen-bonded windmill-like and Saturn-ring-like assemblies of $(HPPD^+)_3(H^+)_2[PMo_{12}O_{40}]^{5-}(CH_3CN)_{3-6}$ (**1**) and $(HTMPPD^+)_6[SiMo_{12}O_{40}]^{6-}(CH_3CN)_6$ (**2**) (Scheme 1) were observed ($HPPD^+$ and $HTMPPD^+$ were the monoprotonated species of PPD and TMPPD).

EXPERIMENTAL SECTION

Instruments, Materials, and Methods. The $(n\text{-}Bu_4N)_3[PMo_{12}O_{40}]^{3-}$ and $(n\text{-}Bu_4N)_4[SiMo_{12}O_{40}]^{4-}$ for the cyclic voltammetry (CV) were prepared by the cation exchange reaction according to the literature.[16] The redox potentials were measured in anhydrous CH_3CN with 0.1 M $(n\text{-}Bu_4N)(BF_4)$ as a supporting electrolyte, using platinum electrodes (working- and counter-electrode) and a saturated calomel electrode (SCE) as reference electrode with a scan rate of 20 mV s^{-1}. The redox titrations of Mo^V in salts **1** and **2** were carried out using a conductance cell of CT-57101B (TOA Electronics Ltd.). The salts **1** and **2** (∼10 mg) were dissolved in dimethylformamide (DMF) - 1 M H_2SO_4 solution, which were titrated by 0.01 N $Ce(SO_4)_2$ solution at 23 °C. During the titration, the potential jumps from about 400 to about 1100 mV were monitored. Infrared (IR, 400−7600 cm^{-1}) spectra measurements were carried out on KBr disks using a Perkin-Elmer Spectrum 2000 spectrophotometer with a resolution of 4 cm^{-1}. UV−vis−NIR spectra (350−3200 nm) were measured on KBr disks using a Perkin-Elmer lambda-19 spectrophotometer with a resolution of 8 nm.

Commercially available *p*-phenylenediamine (PPD) and 2,3,5,6-tetramethyl-PPD (TMPPD) were purified by a vacuum sublimation under the condition of 353 and 363 K at ∼2 Pa, respectively, prior to use. The $(H^+)_3[PMo_{12}O_{40}]^{3-}\cdot nH_2O$ (n = 20) and $(H^+)_4[SiMo_{12}O_{40}]^{4-}\cdot nH_2O$ (n = 20) purchased from Tokyo Kasei Inc. and Sigma-Aldrich Inc., respectively, were used for the crystal growth without further purification. The crystals were grown using a standard diffusion method in a *H*-shaped cell (∼50 mL, Sugiyamagen Corporation). $(H^+)_3[PMo_{12}O_{40}]^{3-}\cdot nH_2O$ (∼100 mg) or $(H^+)_4[SiMo_{12}O_{40}]^{4-}\cdot nH_2O$ (∼100 mg) and PPD (50 mg) or TMPPD (50 mg) were introduced into opposite sides of the *H*-shaped cell (50 mL) and CH_3CN (distilled prior to use) was introduced into the diffusion cell slowly. After 10 days, single crystals with a typical dimension of 0.5 × 0.5 × 0.4 mm^3 were obtained as black-blocks in the $[XMo_{12}O_{40}]$ souse side. Yield of salts **1** and **2** were 22 and 21%, respectively. In the crystal growth of salt **2**, a polymorph was obtained as needle crystals, which have different crystal structure from that of salt **2**.[17] The needle crystals were removed by hand-picking for other experiments. The stoichiometries of the salts **1** and **2** were determined by X-ray structural analysis and elemental analysis as $(HPPD^+)_3(H^+)_2[PMo_{12}O_{40}]^{5-}(CH_3CN)_{3-6}$ (**1**) and $(HTMPPD^+)_6[SiMo_{12}O_{40}]^{6-}(CH_3CN)_6$ (**2**). Elemental analysis of salt **1**: Calcd for $C_{28}H_{44}O_{40}N_{11}PMo_{12}P$: C, 14.26; H, 1.95; N, 6.53. Found. C, 14.25; H, 2.14; N, 6.16. Salt **2**: Calcd for $C_{72}H_{120}O_{40}N_{18}SiMo_{12}$: C, 28.29; H, 3.96; N, 8.25. Found. C, 27.74; H, 3.72; N, 8.10. The solvent number of CH_3CN molecules in salts **1** and **2** were determined by TG-DTA measurement using a Rigaku Thermo Plus TG8120 with a scanning rate of 5 K min^{-1} under N_2 flow. These measurements showed an about 6 and 8% weight-loss of salts **1** and **2** by increasing of the temperatures up to 400 K, which corresponds about 4 and 6 CH_3CN molecules in salts **1** and **2**, respectively. Since the CH_3CN molecules in salt **1** was easily removed from the crystals (see TG analysis), the stoichiometry of $(HPPD^+)_3(H^+)_2[PMo_{12}O_{40}]^{5-}(CH_3CN)_{3-6}$ (**1**) was assumed in the elemental and TG analyses. It should be noted that the mixed-protonated foumula of $(H2PPD^{2+})_2(HPPD^+)[PMo_{12}O_{40}]^{5-}(CH_3CN)_{3-6}$ was also consistent with the elemental and TG analyses.

Crystallography. Crystallographic data (Table 1) were collected by a Rigaku Raxis-Rapid diffractometer using Mo−Kα (λ = 0.71073 Å) radiation from a graphite monochromator. Structure refinements were performed using the full-matrix least-squares method on F^2. Calculations were performed using Crystal Structure software packages.[18] Parameters were refined using anisotropic temperature factors except for the

dx.doi.org/10.1021/ic200683e |*Inorg. Chem.* 2011, 50, 6711–6718

Table 1. Crystal Data, Data Collection, and Reduction Parameters of Crystals 1 and 2 at 100 K

	1	2
chemical formula	$C_{30}H_{45}O_{40}N_{12}PMo_{12}$	$C_{72}H_{120}O_{40}N_{18}SiMo_{12}$
M.W.	2398.01	3057.20
space group	$R\bar{3}$ (no. 148)	$R\bar{3}c(h)$ (no. 167)
a, Å	23.214(4)	28.649(3)
b, Å	10.184(3)	
c, Å	4753(2)	20.480(3)
V, Å^3	4753(2)	14557(3)
Z	3	6
D_{calcd}, g cm^{-1}	2.513	2.092
T (K)	100	100
μ, cm^{-1}	24.147	15.992
reflections measured	21692	75943
independent reflections	2410	3712
reflections used	1750	2755
R_{int}	0.0976	0.0444
R_1[a]	0.0524	0.0982
$wR_2(F^2)$[a]	0.0816	0.0402
GOF	1.173	1.286
ρ_{max}, e$^-$ Å^{-3}	2.27	3.43
ρ_{min}	−1.34	−3.32

[a] $R = \Sigma||F_o| - |F_c||/\Sigma|F_o|$ and $Rw = \{\Sigma w(F_o^2 - F_c^2)^2/\Sigma w(F_o^2)^2\}^{1/2}$.

hydrogen atoms, and these were refined using the riding model with a fixed C−H distance of 0.95 Å.

Solvent Removal. Single crystals of salt **1** were immersed into H_2O, CH_3OH, C_2H_5OH, hexane, CH_2Cl_2 (~10 mL) for 2 min at 296 K. The single crystals were collected by the filtration, then the IR spectra on KBr pellets was measured. The nitrile stretching vibrational mode (ν_{CN}) was monitored before and after immersing of the corresponding solvents.

RESULTS AND DISCUSSION

Crystal Growth and Redox Properties. The *p*-phenylenediamine (PPD) derivatives have strong electron-donating and proton accepting associated with the two amino ($-NH_2$) groups,[19] which are good candidates to form the hydrogen-bonded assemblies with the reduced $[PMo_{12}O_{40}]^{4-}$ and $[SiMo_{12}O_{40}]^{5-}$ clusters. We already reported the crystal structures and magnetic properties of $(PPD)_2([12]crown\text{-}4)_4[PMo_{12}O_{40}]^{4-}$, $(PPD)_4([15]crown\text{-}5)_4[PMo_{12}O_{40}]^{4-}$, and $(PPD)_3([18]crown\text{-}6)_4[PMo_{12}O_{40}]^{4-}$ hybrids, in which the hydrogen-bonding interactions between the protonated PPD and crown ethers were preferentially observed.[20] On the other hand, in the $(Cs^+)_3([18]crown\text{-}6)_3(H^+)_2[PMo_{12}O_{40}]^{5-}$ hybrid, the $Cs^+([18]crown\text{-}6)$ assembly formed through the $Cs^+ \sim O$ interactions.[12] Since the oxygen atoms of crown ethers preferentially form supramolecular assemblies with the cationic species and defines the hydrogen-bonded interactions between the cation and the POM, the direct reaction between PPD derivatives (PPD and tetramethyl-PPD) and $[PMo_{12}O_{40}]^{3-}$ or $[SiMo_{12}O_{40}]^{4-}$ were carried out.

During the reaction the color of the solvent changed from yellow to black-violet as the slow diffusion between $(H^+)_n[XMo_{12}O_{40}]^{n-}$ ($n = 3$ for X = P and $n = 4$ for X = Si) and PPD (or TMPPD) in CH_3CN over 2−3 days proceeded, which then finally resulted in the growth of black-colored single crystals of salts $(HPPD^+)_3(H^+)_2[PMo_{12}O_{40}]^{5-}(CH_3CN)_{3-6}$ (**1**) and $(HTMPPD^+)_6[SiMo_{12}O_{40}]^{6-}(CH_3CN)_6$ (**2**), which were obtained as the two-electron reduced mixed-valence $[XMo_{12}O_{40}]^{(n+2)-}$ salts. It should be noted that the two possible protonated states of $HPPD^+$ and $H2PPD^{2+}$ were assumed in the formula of salt **1**. The redox potentials for the $[PMo_{12}O_{40}]^{3-}$ (or $[SiMo_{12}O_{40}]^{4-}$) and PPD (or TMPPD) were measured by cyclic voltammetry in CH_3CN at 296 K. Reversible two-step one-electron reduction of $[PMo_{12}O_{40}]^{3-}$ were observed at the half-wave reduction potentials of $E^r_{1/2}(1) = +0.186$ and $E^r_{1/2}(2) = -0.251$ V, respectively, while those of $[SiMo_{12}O_{40}]^{4-}$ were observed at $E^r_{1/2}(1) = -0.314$ V and $E^r_{1/2}(2) = -0.723$ V (vs SCE, *n*-Bu_4NBF_4, Pt in CH_3CN). The electron accepting ability of $[PMo_{12}O_{40}]^{3-}$ was about 0.5 V higher than that of $[SiMo_{12}O_{40}]^{4-}$ in CH_3CN, which was consistent with the previous results.[20a,21] Since the $E^r_{1/2}(1)$ values of typical electron-acceptors of 7,7,8,8-tetaracyano-*p*-quinodimethane (TCNQ) was observed at $E_{1/2}(1) = +0.223$ V, the electron accepting strengths of $[PMo_{12}O_{40}]^{3-}$ was almost similar to that of TCNQ. Also, the half-wave first oxidation potentials $[E^o_{1/2}(1)]$ of PPD and TMPPD were observed at +0.299 and +0.146 V, respectively, under the same measurement conditions. The electron-donating ability of TMPPD was about 0.15 V higher than that of PPD because of the existence of electron-donating methyl groups.

The abilities of electron-transfer from PPD (or TMPPD) to $[PMo_{12}O_{40}]^{3-}$ (or $[SiMo_{12}O_{40}]^{4-}$) during the crystallization were estimated from the difference of redox potentials between $E^o_{1/2}(1)$ of PPD (or TMPPD) and $E^r_{1/2}(1)$ of $[PMo_{12}O_{40}]^{3-}$ (or $[SiMo_{12}O_{40}]^{4-}$), $\Delta E = E^o_{1/2}(1) - E^r_{1/2}(1)$.[22] The ΔE values of salts **1** and **2** were 0.113 and 0.460 V, respectively. From the theoretical *V*-shaped diagram by Torrance et al.,[22a] the electronic ground states of donor−acceptor type charge transfer (CT) complexes have been predicted as ionic or neutral from the ΔE values. When the ΔE was larger than about 0.3 V, the neutral electronic ground state was preferable in the CT complex, while the condition of $\Delta E < 0.3$ V yielded the ionic electronic ground state through the full charge transfer from the electron donor to the electron acceptor. The ionic and neutral electronic ground states of salts **1** and **2** were expected from the ΔE values of 0.113 and 0.460 V, respectively. However, it has been reported that the reduction potentials of $[SiMo_{12}O_{40}]^{4-}$ were sensitive to the concentration of the cationic species in CH_3CN.[23] The one-electron reduction wave of $E^r_{1/2}(1)$ changed to the two-electron reduction one by adding the cationic species such as H^+, Li^+, Na^+, and so forth, with about 0.25 V anodic shift of the reduction potential,[22] although such potential shift was not detected in $[PMo_{12}O_{40}]^{3-}$ species in CH_3CN. The anodic shift of $E^r_{1/2}(1)$ of $[SiMo_{12}O_{40}]^{4-}$ resulted in the ionic electronic ground states of $[SiMo_{12}O_{40}]^{6-}$ during the crystallizations of salt **2** as in case of $[PMo_{12}O_{40}]^{5-}$ in salt **1**, which have been confirmed by the redox titrations and electronic spectra.

Two-Electron Reduced $[PMo_{12}O_{40}]^{5-}$ and $[SiMo_{12}O_{40}]^{6-}$ Compounds. The two-electron reduced mixed-valence $[PMo^V{}_2Mo^{VI}{}_{10}O_{40}]^{5-}$ and $[SiMo^V{}_2Mo^{VI}{}_{10}O_{40}]^{6-}$ were confirmed by the redox titrations of salts **1** and **2** at 296 K. The redox titrations (Figure 1a) allowed the determination of the number of Mo^V ions within the cluster. However, the potential jumps that occurred during the redox titration of salts **1** and **2** corresponded to 8 and 14 electrons, respectively (Figure 1a). In these salts, the electron donors PPD and TMPPD in acidic solution also contribute to the redox titration as a consequence of $PPD \rightarrow PPD^+ + e^- \rightarrow PPD^{2+} + e^-$ (or $TMPPD \rightarrow TMPPD^+ + e^- \rightarrow TMPPD^{2+} + e^-$). However, the stoichiometries of $(PPD)_3[PMo_{12}O_{40}]^{5-}$ and $(TMPPD)_6[SiMo_{12}O_{40}]^{6-}$ are consistent

dx.doi.org/10.1021/ic200683e |*Inorg. Chem.* 2011, 50, 6711–6718

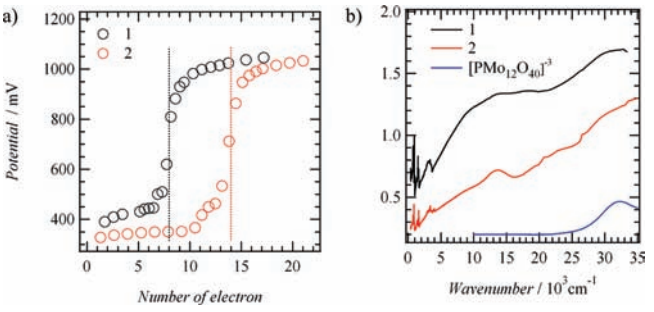

Figure 1. Electronic ground states of $[PMo_{12}O_{40}]^{5-}$ and $[SiMo_{12}O_{40}]^{6-}$ in salts **1** and **2**. (a) Redox titrations of salts **1** and **2** in DMF - 1 M H_2SO_4 solution using Ce(III) ion at 296 K. (b) Solid state electronic spectra of salts **1** and **2** in KBr pellets together with solution spectrum of $H_3^+[PMo_{12}O_{40}]^{3-}$ in CH_3CN.

with the 8 and 14 electrons respectively, that is, the oxidation process of 3PPD + $2Mo^V$ (8 electrons) and 6TMPPD + $2Mo^V$ (14 electrons), respectively.

The mixed-valence electronic states of $[PMo_{12}O_{40}]^{5-}$ and $[SiMo_{12}O_{40}]^{6-}$ in salts **1** and **2** were confirmed by UV−vis−NIR−IR spectra of the solid (Figure 1b), and the yellow-colored $(H^+)_3[PMo_{12}O_{40}]^{3-}$ did not show the d−d transition (blue line in Figure 1b) because of the $(4d)^0$ electronic state of the Mo^{VI} ions. Also, the electronic absorptions at 32 and 46 × 10^3 cm^{-1} can be assigned to metal-ligand charge transfer electronic excitation from the doubly occupied oxo-orbitals to unoccupied d-orbitals of Mo^{VI}.[24] On the other hand, the electronic spectra of salts **1** and **2** show a broad absorption in the vis−NIR−IR energy region, and the octahedral coordination of the six oxygen atoms to a Mo^V ion split in an octahedral field, that is, the d-orbitals are divided into t_{2g}- and e_g-orbitals, whose energy separation is usually larger than 10 × 10^3 cm^{-1}. Therefore, the low energy electronic absorption in salts **1** and **2** at ∼8 × 10^3 cm^{-1} was assigned to the intervalence transition from the Mo^V to Mo^{VI} ions through the Mo−O−Mo bond within the cluster,[24] and the bands at ∼12 and ∼18 × 10^3 cm^{-1} were observed in the typical energy region of the d−d transitions of Mo^V ion.

Vibrational Spectra of Salts 1 and 2. From the elemental analysis and X-ray crystal structural analysis, the stoichiometries of salts **1** and **2** were determined to be $(HPPD^+)_3(H^+)_2[PMo_{12}O_{40}]^{5-}(CH_3CN)_{3-6}$ (**1**) and $(HTMPPD^+)_6[SiMo_{12}O_{40}]^{6-}(CH_3CN)_6$ (**2**), respectively. To compensate the total charge within the crystals, the PPD and TMPPD must be protonated, and the vibrational spectra of salts **1** and **2** were useful to confirm the protonated states of PPD and TMPPD molecules; thus we evaluated the N−H stretching vibrational modes (ν_{N-H}) and the N−H deformation modes (δ_{N-H}) of $-NH_2$ and $-NH_3^+$ in salts **1** and **2** (see Supporting Information, Figure S2). The ν_{N-H} modes of $-NH_2$ and $-NH_3^+$ have been typically observed at 3500−3300 cm^{-1} and 3130−3030 cm^{-1}, respectively, while the δ_{N-H} modes of $-NH_2$ and $-NH_3^+$ were observed at around 1650−1560 cm^{-1} and 1600 cm^{-1}, respectively.[25] The ν_{N-H} modes of $-NH_2$ group in salts **1** and **2** were observed as broad band around 3400 cm^{-1}, while the ν_{N-H} modes of $-NH_3^+$ group of salts **1** and **2** were confirmed as a broad band with absorption maxima at 3052 and 2050 cm^{-1}, respectively. In the δ_{N-H} energy region, two δ_{N-H} bands in both of the salts **1** and **2** were observed around 1630 and 1600 cm^{-1}, corresponding to the $-NH_2$ and $-NH_3^+$ groups, respectively.

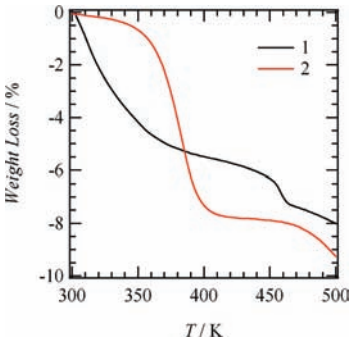

Figure 2. TG diagram of salts **1** and **2**.

Therefore, protonated PPD derivatives of $HPPD^+$ and $HTMPPD^+$ existed in salts **1** and **2** from the cation−anion ratio and the crystal structures. Since the quantitative analysis for the amount of monoprotonated $HPPD^+$ and diprotonated $H2PPD^{2+}$ was difficult in IR spectra, we could not remove the crystal formula of mixed-protonated $(H2PPD^{2+})(HPPD^+)_3[PMo_{12}O_{40}]^{5-}(CH_3CN)_{3-6}$ instead of $(HPPD^+)_3(H^+)_2[PMo_{12}O_{40}]^{5-}(CH_3CN)_{3-6}$.

Thermal Stabilities of Salts 1 and 2. Temperature dependent thermogravity (TG) diagrams (Figure 2) revealed the thermal stabilities of salts **1** and **2**. Since the hydrogen-bonding ionic structures between the PPD derivatives and $[XMo_{12}O_{40}]^{(n+2)-}$ should be relatively stable, the weight-loss during the TG analyses is dominated by the acetonitrile solvent. The weight-loss of 7.8% in salt **2** was observed by increasing of the temperature up to 450 K, whose magnitude is consistent with the presence of six CH_3CN molecules (calcd. 8.1%). The weight-loss of salt **2** started around 350 K, indicating that the salt **2** was thermally stable up to about 350 K. On the contrary, rapid weight-loss of salt **1** occurred around room temperature, which reached at about 6% around 450 K, and the weight-loss of ∼6% was much smaller than that for six CH_3CN molecules (10.2%), indicating that two or three CH_3CN molecules were already removed from the salt **1** before the start of TG measurement, that is, $(HPPD^+)_3(H^+)_2[PMo_{12}O_{40}]^{5-}(CH_3CN)_{3-6}$, the magnitude of weight-loss for three CH_3CN molecules (5.3%) was well consistent with the experimental result. The difference of thermal stabilities between the salts **1** and **2** can be explained by the dimensionality of nanospaces in the crystal occupied by solvent molecules (see Packing Structures). From the redox titration, optical measurements, TG analysis, and X-ray crystal structural analysis, the stoichiometries of salts **1** and **2** were assumed as $(HPPD^+)_3(H^+)_2[PMo_{12}O_{40}]^{5-}(CH_3CN)_{3-6}$ (**1**) and $(HTMPPD^+)_6[SiMo_{12}O_{40}]^{6-}(CH_3CN)_6$ (**2**), respectively.

Packing Structure. In salts **1** and **2**, the formation of α-Keggin structures was observed which crystallized in the space group of $R\bar{3}$ and $R\bar{3}c$ for salts **1** and **2**, respectively. The $[PMo_{12}O_{40}]^{5-}$ clusters are arranged hexagonally within the *ab*-plane (Figure 3a) connected through hydrogen-bonded interactions to each other, where the $[PMo_{12}O_{40}]^{5-}$ clusters exists alternately above and below in the *ab*-plane (Figure 3b). The infinite N−H ∼ O hydrogen-bonding interactions between the $[PMo_{12}O_{40}]^{5-}$ and $HPPD^+$ (or $H2PPD^{2+}$) effectively constructed the three-dimensional assembly structure of mixed-valence $[PMo_{12}O_{40}]^{5-}$. The intercluster interaction between the $[PMo_{12}O_{40}]^{5-}$ in the *ab*-plane was negligible because of the long P−P distances (d_{P-P}) of 13.80 Å, while relatively short d_{P-P} of 10.12 Å was

dx.doi.org/10.1021/ic200683e |*Inorg. Chem.* 2011, 50, 6711–6718

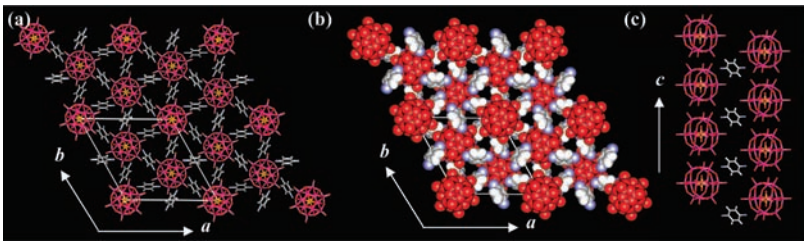

Figure 3. Packing structure of salt **1**. (a) Unit cell viewed along the *c*-axis. (b) Space filling representation of the assembly, where the one-dimensional channels elongated along the *c*-axis. The CH_3CN molecules were omitted to clarify the figure. (c) One-dimensional $[PMo_{12}O_{40}]^{5-}$ arrangement along the *c*-axis, where the shortest $O_a \sim O_b$ distance of 3.009(9) Å was observed.

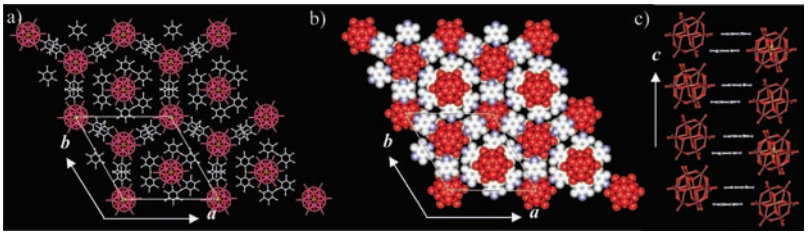

Figure 4. Packing structure of salt **2**. (a) Unit cell viewed along the *c*-axis. The CH_3CN molecules are omitted to clarify the figure. (b) Space filling representation of $(TMPPD)_6[SiMo_{12}O_{40}]^{6-}$ assembly viewed along the *c*-axis. (c) One-dimensional $[SiMo_{12}O_{40}]^{6-}$ arrangement along the *c*-axis were connected by the N−H ∼ O hydrogen-bonding and the $\pi-\pi$ stacking interactions. Between the π-dimer of TMPPD molecules, two CH_3CN molecules existed in the antiparallel arrangement.

observed along the *c*-axis (Figure 3c). Along the *c*-axis, each $[PMo_{12}O_{40}]^{5-}$ directly interacted through the interatomic O_a-O_b distance of 3.009(9) Å.

The space filling representation of the $(HPPD^+)_3(H^+)_2[PMo_{12}O_{40}]^{5-}$ assembly shown in Figure 3b shows one-dimensional triangular spaces which are elongated along the *c*-axis, where the CH_3CN solvent molecules are occupied. The cross-sectional area of the nanospace was about 0.065 nm^2, and its surface is surrounded by the π-plane of $HPPD^+$ and the terminal $Mo{=}O_b$ oxygen atoms of $[PMo_{12}O_{40}]^{5-}$. From the TG experiments, it was shown that the CH_3CN molecules are easily released from the crystal, even at room temperature. The CH_3CN molecules present in the one-dimensional channels are easily removed by immersing the single crystals into H_2O, CH_3OH, and C_2H_5OH (see the section on Solvent Removal), suggesting that hydrophilic molecular recognition environments are present in the crystal.

Figure 4 shows the packing structure of salt **2**. The hydrogen-bonding $(HTMPPD^+)_6[SiMo_{12}O_{40}]^{6-}$ assembly further formed the π-stacking interaction between the TMPPD molecules. In the *ab*-plane, the hexagonal $[SiMo_{12}O_{40}]^{6-}$ arrangement was observed through the N2−H ∼ O hydrogen-bonded interactions, that is, the hydrogen-bonding Saturn-ring-like assemblies of $(TMPPD)_6[SiMo_{12}O_{40}]^{6-}$ were further connected infinitely within the *ab*-plane. The nearest-neighboring intercluster Si−Si distance (d_{Si-Si}) of 16.89 Å in the *ab*-plane indicated the independent cluster arrangement, while the effective intercluster interaction of d_{Si-Si} of 10.25 Å was observed along the *c*-axis. Along the *c*-axis, the shortest $O_a \sim O_b$ distance of 3.060(8) Å was observed between the $[SiMo_{12}O_{40}]^{6-}$ (see Supporting Information, Figure S8), which distance was similar to that in salt **1** (d_{O-O} = 3.009 Å). The $HTMPPD^+$ molecules formed the π-stacking dimer with a mean interplanar distance of 3.3 Å (Figure 4c). Between the π-dimer stacks (Figure 4c), two CH_3CN molecules arranged in the antiparallel manner to cancel the dipole moments. The CH_3CN molecules surrounding by

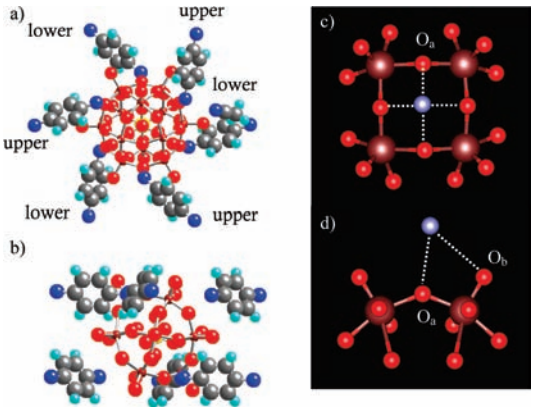

Figure 5. Hydrogen-bonding PPD − $[PMo_{12}O_{40}]^{5-}$ assembly in salt **1**. (a, b) Windmill-like $(PPD)_6[PMo_{12}O_{40}]^{5-}$ assembly. (c, d) Hydrogen-bonding sites between the nitrogen atom of PPD and the bridging O_a and terminal O_b oxygen atoms of $[PMo_{12}O_{40}]^{5-}$. Blue, red, brown, and gray spheres are nitrogen, oxygen, molybdenum, and carbon atoms, respectively.

TMPPD molecules could not be easily released from the crystals, which was consistent with higher thermal stability of salt **2** than that of salt **1**.

Hydrogen-Bonding Assemblies in Salts 1 and 2. The hydrogen-bonding assemblies in salts **1** and **2** were characterized by the X-ray crystal structural analyses. In the Keggin cluster, two kinds of oxygen atoms (24 metal-bridging $Mo-O_a-Mo$ and 12 terminal $Mo{=}O_b$ in Scheme 1) can contribute to the intermolecular hydrogen-bonds. It has been reported that the acidic protons in $(H^+)_3[PMo_{12}O_{40}]^{3-}$ cluster were located at the bridging $Mo-O_a-Mo$ oxygen atomic sites from the Electron Nuclear Double Resonance (ENDOR)-NMR and density functional theory (DFT) calculations,[26] suggesting that the O_a oxygen atoms have higher hydrogen-bonding ability than that of O_b ones.

dx.doi.org/10.1021/ic200683e |*Inorg. Chem.* 2011, 50, 6711–6718

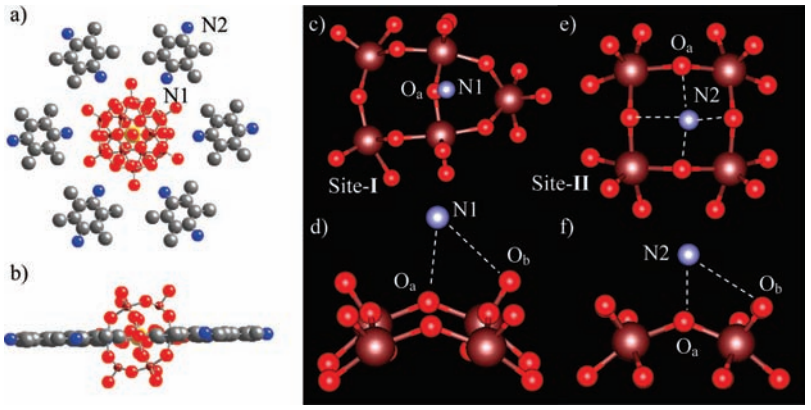

Figure 6. Hydrogen-bonding TMPD − $[SiMo_{12}O_{40}]^{6-}$ assembly in salt **2**. (a, b) Hydrogen-bonding Saturn-ring-like $(TMPPD)_6[SiMo_{12}O_{40}]^{6-}$ assembly, where the hydrogen atoms were omitted in figure. Two kinds of hydrogen-bonding interactions of N1 ∼ O_a and N2 ∼ O_a were defined as site-**I** (c and d) and site-**II** (e and f), respectively. Blue, red, brown, and gray spheres are nitrogen, oxygen, molybdenum, and carbon atom, respectively.

Figures 5a and 5b show the hydrogen-bonded $(PPD)_6[PMo_{12}O_{40}]^{5-}$ assembly in salt **1**. The $[PMo_{12}O_{40}]^{5-}$ cluster was surrounded by the six protonated PPD molecules ($HPPD^+$ or $H2PPD^{2+}$), forming a windmill-like assembly and six PPD molecules arranged alternately at the upper and lower position of $[PMo_{12}O_{40}]^{5-}$ through the N−H ∼ O hydrogen-bonding interactions (Figure 5a and Figure 5b). The dihedral angle of the nearest-neighboring mean π-planes of PPD was 60 degrees, and the interacting nitrogen atom of PPD exists at a central position of four bridging Mo−O_a−Mo oxygen atoms (Figure 5c), where the N−O_a distances of 2.894(8), 2.905(6), 3.073(6), and 3.078(9) Å were about 1 Å shorter than the N−O_b distance of 3.95 Å (Figure 5d), suggesting that dominant intermolecular interactions occurred at the N ∼ O_a hydrogen-bonds. From the charge-state of $[PMo_{12}O_{40}]^{5-}$ and stoichiometry of salt **1**, five protons are necessary to compensate the total charge of the crystal. To distinguish between the $-NH_2$ and $-NH_3^+$ sites of PPD was quite difficult because of the crystal symmetry of the equivalent nitrogen atomic sites of PPD. Two possible protonated states of PPD in salt **1** were $(HPPD^+)_3(H^+)_2[PMo_{12}O_{40}]^{5-}$ and $(H2PPD^{2+})_2(HPPD^+)[PMo_{12}O_{40}]^{5-}$, in which the average structure of N−H^+ ∼ O and N−H ∼ O hydrogen bonding interactions was observed in the X-ray crystal structural analysis.

The molecular-assembly of $(HTMPD^+)_6[SiMo_{12}O_{40}]^{6-}$ in salt **2** was constructed from six N−H ∼ O hydrogen bonding interactions between the oxygen atoms of $[SiMo_{12}O_{40}]^{6-}$ and nitrogen atoms of TMPD (Figure 6a and Figure 6b). The π-planes of $HTMPPD^+$ were parallel to each other, forming a Saturn-ring-like molecular-assembly. In salt **2**, one $HTMPPD^+$ molecule was the crystallographically independent unit, where two nitrogen atoms (N1 and N2) had a different hydrogen-bonding environment (site-**I** and site-**II**). The hydrogen-bonds at the site-**I** and site-**II** corresponded to the N1−H ∼ O and the N2−H ∼ O interactions, respectively, and the site-**I** was observed around the $[SiMo_{12}O_{40}]^{6-}$ cluster. The hydrogen-bonding at site-**II** connected each Saturn-ring infinitely within the *ab*-plane (see Figure 4a). In the site-**I**, the N1−O_a distance of 3.084 Å was slightly shorter than the N1−O_b distance of 3.163 Å. On the other hand, since the N2−O_a distances of 2.783(12), 2.835(12), 2.993(9), and 3.061(7) Å in site-**II** were much shorter than the N2−O_b distance of 4.049(10) Å (the hydrogen-bonding at O_b site is of negligible magnitude).

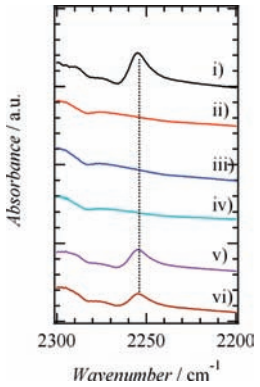

Figure 7. Vibrational spectra of salt **1** in the frequency range from 2300−2200 in KBr pellets. The spectra of (i) initial state of salt **1** and after immersion of the single crystals into (ii) CH_3OH, (iii) H_2O, (iv) C_2H_5OH, (v) CH_2Cl_2, and (vi) hexane.

From the crystal stoichiometry and vibrational spectra, the protonated state of $HTMPPD^+$ should be reasonable ones in $(HTMPPD^+)_6[SiMo_{12}O_{40}]^{6-}(CH_3CN)_6$. We evaluated the N−C bond distances of TMPPD to distinguish the type of C-NH_2 and C-NH_3^+ bonds. It has been reported that the C−NH_3^+ bond length for the ammonium site is longer than the C−NH_2 one for the amino site.[12] Since the N1−C1 = 1.395(9) Å of TMPPD (site-**I**) was about 0.5 Å longer than the N2−C4 = 1.443(9) Å (site-**II**), the NH_3^+ ∼ O and NH_2 ∼ O hydrogen-bonding sites could be safely assigned to the site-**I** and site-**II**, respectively. Therefore, six ionic $-NH_3^+$ ∼ O hydrogen-bonding interactions around the $[SiMo_{12}O_{40}]^{6-}$ formed the Saturn-ring-like assembly to reduce the electrostatic interactions.

Solvent Remove from Salt 1. The one-dimensional channels of salt **1** were occupied by CH_3CN molecules, whose removal in H_2O, CH_3OH, C_2H_5OH, CH_2Cl_2, and hexane was evaluated at 296 K. The solvent removal was monitored by vibrational spectra. Although the overall spectral features were the same before and after immersing of the single crystals into the solvent, the nitrile stretching mode (ν_{CN}) of CH_3CN disappeared by the immersion of the single crystals into CH_3OH (ii), H_2O (iii), and C_2H_5OH (iv in Figure 7), indicating the removal of CH_3CN. When the crystals were immersed into CH_2Cl_2 (v) and hexane (vi), the ν_{CN} modes remained unchanged, suggesting no solvent

dx.doi.org/10.1021/ic200683e |*Inorg. Chem.* 2011, 50, 6711–6718

removal reaction. Since the one-dimensional channel surrounded by PPD molecules and terminal Mo=O_b oxygen atoms formed the hydrophilic channel, small size polar molecules such as H_2O and CH_3OH were responsible for the solvent remove reaction. Such phenomena were not detected in salt **2**, and is consistent with high thermal stability of salt **2** in the TG analysis.

CONCLUSIONS

The electron-transfer and proton-transfer reactions between the electron-donor (proton-acceptor) of PPD derivatives and the electron-acceptor (proton-donor) of $(H^+)_3[XMo_{12}O_{40}]^{n-}$ (n = 3 for X =P and n = 4 for X = Si) in the crystallization solvent (CH_3CN) resulted in new mixed-valence salts of $(HPPD^+)_3(H^+)_2[PMo_{12}O_{40}]^{5-}(CH_3CN)_{3-6}$ (**1**) and $(HTMPD^+)_6[SiMo_{12}O_{40}]^{6-}(CH_3CN)_6$ (**2**). The electrostatic and hydrogen-bonding interactions between the PPD (or TMPPD) and $[PMo_{12}O_{40}]^{5-}$ (or $[SiMo_{12}O_{40}]^{6-}$) play an important role to construct the molecular assemblies of windmill-like and Saturn-ring-like structures in salts **1** and **2**. The electronic ground states of two-electron reduced $[PMo_{12}O_{40}]^{5-}$ and $[SiMo_{12}O_{40}]^{6-}$ were confirmed by the redox titration and electronic spectra and the one-dimensional channel structure surrounding the PPD molecules in salt **1**, which was occupied by the CH_3CN molecules. The initial CH_3CN was removable by immersing of the single crystals into the H_2O, CH_3OH, and C_2H_5OH solvents. Further, the CH_3CN molecules in salt **2** existed in the isolated zero-dimensional crystalline nanospaces, showing a high thermal stability, and the construction of unique two- or three-dimensional molecular-assemblies, utilizing the electron-rich mixed-valence Keggin cluster, have potential to form novel electrical and magnetic materials responsive to the outer chemical stimuli such as molecular sorption and desorption.

ASSOCIATED CONTENT

Supporting Information. Atomic numbering scheme of structural analysis of salts **1** and **2** (CIF), IR and Raman spectra. This material is available free of charge via the Internet at http://pubs.acs.org.

AUTHOR INFORMATION

Corresponding Author

*Phone: +81-22-217-5653 (T.A.). Fax: +81-22-217-5655 (T.A.). E-mail: akuta@tagen.tohoku.ac.jp (T.A.).

ACKNOWLEDGMENT

This work was partly supported by a Grant-in-Aid for Science Research from the Ministry of Education, Culture, Sports, Science and Technology of Japan.

REFERENCES

(1) (a) *Supramolecular Assembly via Hydrogen Bonds I and II*; Mingous, D. M. P., Ed.; Springer-Verlag: Berlin, Germany, 2003. (b) Prins, L. J.; Reinhoudt, D. N.; Timmermane, P. *Angew. Chem., Int. Ed.* **2001**, *40*, 2382. (c) Steiner, T. *Angew. Chem., Int. Ed.* **2002**, *41*, 48. (d) Stephen, L. F. H.; Nuckolls, C. C.; Rebek, J., Jr. *Angew. Chem., Int. Ed.* **2002**, *41*, 1488.

(2) (a) Jeffrey, G. A. *An Introduction to Hydrogen Bonding*; Truhlar, D. G.; Ed.; Oxford University Press: New York, 1997. (b) MacDonald, J. C.; Whitesides, G. M. *Chem. Rev.* **1994**, *94*, 2383. (c) Desiragu, G. *Acc. Chem. Res.* **2002**, *35*, 565.

(3) (a) West, A. R. *Basic Solid State Chemistry*; John Wiley & Sons: New York, 1988. (b) Rodgers, G. E. *Descriptive Inorganic, Coordination, and Solid-State Chemistry*; 2nd ed.; Brooks/Cole Thomson Learning: Pacific Grove, CA, 2002.

(4) (a) *Polyoxometalate Molecular Science*; Borrás-Almenar, J. J., Coronado, E., Müller, A., Pope, M., Eds.; Kluwer Academic Publishers: London, England, 2001. (b) *Polyoxometalate Chemistry From Topology via Self-Assembly to Applications*; Pope, T., Müller, A., Eds.; Kluwer Academic Publishers: London, England, 2001. (c) *Polyoxometalate Chemistry for Nano-Composite Design*; Yamase, T., Pope, M. T., Eds.; Kluwer Academic Publishers: New York, 2002. (d) Cronin, L. In *Comprehensive Coordination Chemistry II*; Elsevier-Pergamon: New York, 2004; Vol. 7, p 1.

(5) (a) Song, Y.-F.; Abbas, H.; Ritchie, C.; McMillian, N.; Long, D.-L.; Gadegaard, N.; Cronin, L. *J. Mater Chem.* **2007**, *17*, 1903. (b) Wilson, E. F.; Abbas, H.; Duncombe, B. J.; Streb, C.; Long, D.-L.; Cronin, L. *J. Am. Chem. Soc.* **2008**, *130*, 13876. (c) Abbas, H.; Streb, C.; Pickering, A. L.; Neil, A. R.; Long, D.-L.; Cronin, L. *Cryst. Growth Des.* **2008**, *8*, 635.

(6) (a) Gaunt, A. J.; May, I.; Collison, D.; Fox, O. D. *Inorg. Chem.* **2003**, *42*, 5049. (b) Ishii, Y.; Takenaka, Y.; Konishi, K. *Angew. Chem., Int. Ed.* **2004**, *43*, 2702. (c) Zheng, P.; Ren, Y.; Long, L.; Huang, R.; Zheng, L. *Inorg. Chem.* **2005**, *44*, 1190. (d) Gamelas, J. A. F.; Santos, F. M.; Felix, V.; Cavaleiro, A. M. V.; De Matos Gomes, E.; Belsley, M.; Drew, M. G. B. *Dalton Trans.* **2006**, 1197. (e) Chang, S.; Qin, C.; Wang, E.; Li, Y.; Wang, X. *Inorg. Chem. Commun.* **2006**, *9*, 727. (f) Chiba, H.; Wada, A.; Ozeki, T. *Dalton Trans.* **2006**, 1213.

(7) (a) Niu, J.; Wei, M.; Wang, J. *J. Mol. Struct.* **2004**, *689*, 147. (b) Niu, J.; Wei, M.; Wang, J.; Dang, D. *Eur. J. Chem.* **2004**, 160. (c) Dai, L.; Wang, E.; You, W.; Zhang, Z. *J. Cluster Sci.* **2008**, *19*, 511. (d) Tian, A.; Ying, J.; Peng, J.; Sha, J.; Pang, H.; Zhang, P.; Chen, Y.; Zhu, M.; Su, Z. *Cryst. Growth Des.* **2008**, *8*, 3717. (e) Dai, L.; You, W.; Wang, E.; Wu, S.; Su, Z.; Du, Q.; Zhao, Y.; Fang, Y. *Cryst. Growth Des.* **2009**, *9*, 2110.

(8) (a) Ren, Y.; Kong, X.; Hu, X.; Sun, M.; Long, L.; Huang, R.; Zheng, L. *Inorg. Chem.* **2006**, *45*, 4016. (b) Kong, X.; Ren, Y.; Zheng, P.; Long, Y.; Long, L.; Huang, R.; Zheng, L. *Inorg. Chem.* **2006**, *45*, 10702. (c) Zhai, Q.; Wu, X.; Chen, S.; Chen, L.; Lu, C. *Inorg. Chim. Acta* **2007**, *360*, 3484. (d) Wang, X.; Qin, C.; Wang, E.; Su, Z. *Chem. Commun.* **2007**, 4245. (e) Yuan, L.; Qin, C.; Wang, X.; Wang, E.; Chang, S. *Eur. J. Inorg. Chem.* **2008**, 4936.

(9) (a) Uchida, S.; Mizuno, N. *Chem.—Eur. J.* **2003**, *9*, 5850. (b) Uchida, S.; Mizuno, N. *J. Am. Chem. Soc.* **2004**, *126*, 1602. (c) Uchida, S.; Kawamoto, R.; Akatsuka, T.; Hikichi, S.; Mizuno, N. *Chem. Mater.* **2005**, *17*, 1367. (d) Jiang, C.; Lesbani, A.; Kawamoto, R.; Uchida, S.; Mizuno, N. *J. Am. Chem. Soc.* **2006**, *128*, 14240. (d) Uchida, S.; Kawamoto, R.; Mizuno, N. *Inorg. Chem.* **2006**, *45*, 5136. (e) Uchida, S.; Noritaka, M. *Coord. Chem. Rev.* **2007**, *251*, 2537. (f) Uchida, S.; Kawamoto, R.; Tagami, H.; Nakagawa, Y.; Mizuno, N. *J. Am. Chem. Soc.* **2008**, *130*, 12370. (g) Lesbani, A.; Kawamoto, R.; Uchida, S.; Mizuno, N. *Inorg. Chem.* **2008**, *47*, 3349. (h) Wang, X.; Bi, Y.; Chen, B.; Lin, H.; Liu, G. *Inorg. Chem.* **2008**, *47*, 2442. (i) Breen, J. M.; Schmitt, W. *Angew. Chem., Int. Ed.* **2008**, *47*, 6904.

(10) (a) Ouahab, L.; Bencharif, M.; Mhanni, A.; Pelloquin, D.; Halet, J.-F.; Peña, O.; Padiou, J.; Grandjean, D.; Garrigou-Lagrange, C.; Amiell, J.; Delhaes, P. *Chem. Mater.* **1992**, *4*, 666. (b) Gómez-Garcia, C. J.; Ouahab, L.; Gimenéz-Saiz, C.; Triki, S.; Coronado, E.; Delhaès, P. *Angew. Chem., Int. Ed.* **1994**, *33*, 223. (c) Galan-Mascarós, J. R.; Gimenéz-Saiz, C.; Triki, S.; Gómez-Garcia, J.; Coronado, E.; Ouahab, L. *Angew. Chem., Int. Ed.* **1995**, *34*, 1460. (d) Bellitto, C.; Bonamico, M.; Fares, V.; Federici, F.; Righini, G.; Kurmoo, M.; Day., P. *Chem. Mater.* **1995**, *7*, 1475. (e) Coronado, E.; Galan-Mascarós, J. R.; Gimenéz-Saiz, C.; Gómez-Garcia, C. J.; Triki, S. *J. Am. Chem. Soc.* **1998**, *120*, 4671. (f) Coronado, E.; Gómez-Garcia, C. J. *Chem. Rev.* **1998**, *98*, 273. (g) Nyman, M.; Ingersoll, D.; Singh, S.; Bonhomme, F.; Alam, T. M.; Brinker, C. J.; Rodriguez, M. A. *Chem. Mater.* **2005**, *17*, 2885.

(11) (a) Neier, R.; Trojanowski, C.; Mattes, R. *J. Chem. Soc., Dalton Trans.* **1995**, 2521. (b) Dolbecq, A.; Lisnard, L.; Mallard, A.; Marrot, J.; Secheresse, F. *Angew. Chem., Int. Ed.* **2002**, *41*, 2398.

(12) Akutagawa, T.; Endo, D.; Kudo, F.; Noro, S.; Takeda, S.; Cronin, L.; Nakamura, T. *Cryst. Growth Des.* **2006**, *8*, 812.

(13) (a) Gamelas, A. F.; Santos, F. M.; Felix, V.; Cavaleiro, A. M. V.; de Matos Gomes, V.; Belsley, M.; Drew, M. G. B. *Dalton. Trans.* **2006**, 1197. (b) Huang, Y.; Chen, J.; Lan, T.; Lu, X.; Wei, C.; Li, Z.; Zhang, Z. *J. Mol. Struct.* **2006**, *783*, 168. (c) Yang, J.; Huang, K.; Pu, Z.; Gong, Y.; Li, H.; Hu, C. *J. Mol. Struct.* **2006**, *789*, 162. (d) Alizadeh, M. H.; Holman, K. T.; Mirzaei, M.; Razavi, H. *Polyhedron* **2006**, *25*, 1567.

(14) (a) Prados, R. A.; Meiklejohn, P. T.; Pope, M. T. *J. Am. Chem. Soc.* **1974**, *96*, 1261. (b) Prados, R. A.; Pope, M. T. *Inorg. Chem.* **1976**, *15*, 2547. (c) Sanchez, C.; Livage, J.; Launary, J. P.; Fournier, M.; Jeannin, Y. *J. Am. Chem. Soc.* **1982**, *104*, 3194.

(15) Suaud, N.; Gaita-Ariño, A.; Clemente-Juan, J. M.; Coronada, E. *Chem.—Eur. J.* **2004**, *10*, 4041.

(16) (a) Prados, R. A.; Meiklejohn, P. T.; Pope, M. T. *J. Am. Chem. Soc.* **1974**, *96*, 1261. (b) Rocchiccioli-Deltcheff, C.; Fournier, M.; Franck, R.; Thouvenot, R. *Inorg. Chem.* **1983**, *22*, 207.

(17) X-ray data for the needle crystal. Tetragonal, a = 22.055(7), c = 12.306(4), V = 5986(3).

(18) (a) *Crystal Structure*, single crystal structure analysis software, Ver. 3.6; . Rigaku Corporation and Molecular Structure Corporation: The Woodlands, TX, 2004. (b) Sheldrick, G. M. *SHELXL93/97*; University of Göttingen: Göttingen, Germany, 1993/1997/2001.

(19) (a) *Handbook of Chemistry and Physics*, 83rd ed.; CRC Press: New York, 2002. (b) Matsunaga, Y.; Osawa, E.; Osawa, R. *Bull. Chem. Soc. Jpn.* **1975**, *48*, 37.

(20) (a) Akutagawa, T.; Endo, D.; Imai, H.; Noro, S.; Cronin, L.; Nakamura, T. *Inorg. Chem.* **2006**, *45*, 8626. (b) Akutagawa, T.; Endo, D.; Noro, S.; Cronin, L.; Nakamura, T. *Coord. Chem. Rev.* **2007**, *251*, 2547.

(21) (a) Sadakane, M.; Steckhan, E. *Chem. Rev.* **1998**, *98*, 219. (b) Himeno, S.; Takamoto, M.; Santo, R.; Ichimura, A. *Bull. Chem. Soc. Jpn.* **2005**, *78*, 95.

(22) (a) Torrance, J. B.; Vazquez, J. E.; Mayerle, J. J.; Lee, V. Y. *Phys. Rev. Lett.* **1981**, *26*, 253. (b) Saito, G.; Ferraris, J. P. *Bull. Chem. Soc. Jpn.* **1980**, *53*, 2142.

(23) Himeno, S.; Takamoto, M.; Ueda, T. *J. Electroanal. Chem.* **2000**, *485*, 49.

(24) (a) Pope, M. T. *Heteropoly and Isopoly Oxometalates*; Springer-Verlag: Berlin, Germany, 1983; p 109. (b) Robin, M. B.; Day., P. *Adv. Inorg. Chem. Radiochem.* **1967**, *10*, 248.

(25) Akalin, E.; Akyüz, S. *Vib. Spectrosc.* **2000**, *22*, 3.

(26) (a) Day, V. W.; Klemperer, W. G.; Maltbie, D. J. *J. Am. Chem. Soc.* **1987**, *109*, 2991. (b) Ganapathy, S.; Fournier, M.; Paul, J. F.; Delevoye, L.; Guelton, M.; Amoureux, J. P. *J. Am. Chem. Soc.* **2002**, *124*, 7821. (c) Janik, M. J.; Davis, R. J.; Neurock, M. *J. Am. Chem. Soc.* **2005**, *127*, 5238.